Modeling 1-D Isothermal Shape Memory Alloy Microstructure via Legendre Wavelets Collocation Method

He , X., Wang, D., Wang, L., and Melnik, R.

In: Proceedings of the 1st International Conference on Numerical Modelling in Engineering. Volume 2: Numerical Modelling in Mechanical and Materials Engineering, NME 2018, Abdel Wahab M. (ed) (28-29 August 2018, Ghent University, Belgium). Lecture Notes in Mechanical Engineering. Springer, pp. 104-113, 2019.

Modeling 1-D Isothermal Shape Memory Alloy Microstructure via Legendre Wavelets Collocation Method

Xuan He[1], Dan Wang[1], Linxiang Wang[1(✉)], and Roderick Melnik[2]

[1] State Key Laboratory of Fluid Power and Mechatronic Systems, Zhejiang University, Hangzhou 310027, China
wanglx236@zju.edu.cn
[2] MS2 Discovery Interdisciplinary Research Institute, Wilfrid Laurier University, Waterloo ON N2L 3L5, Canada

Abstract. Microstructure plays a significant role in the research of shape memory alloy (SMA). Using mathematical modeling tools to study microstructures can predict the behaviors of material under applied fields. In the current paper, a 1-D dynamic isothermal model is proposed to simulate the microstructure of SMA via Legendre wavelets collocation method. Because of the good performance of Legendre wavelets basis, this method shows good properties in both precision and stability. This paper gives a detailed numerical algorithm and employs the backward differentiation formula to perform all simulations. Computational simulations are carried out in both static and dynamic systems to study the stress induced phase transformation (PT). Numerical experiments are performed using different grids in this paper to demonstrate the advantages of reduced computing cost of the proposed method. In addition, good convergence of the method is well illustrated by the numerical results. The microstructure of SMA is well captured in the current paper.

Keywords: Legendre wavelets · Shape memory alloy · Microstructure
Phase transformation

1 Introduction

Since its discovery in the last century [1, 2], SMA has been wildly studied due to the unique mechanical properties, such as shape memory effect and pseudoelasticity. In order to fulfil the application requirements of SMA [3–5], modeling the microstructures of SMA is a major challenge for researchers to study. These studies can be mainly divided into two parts by numerical methods: finite element method and spectral method. Finite element method is wildly applied in the materials simulations. Lagoudas did an excellent job in modeling SMA behaviors via finite element analysis, which can be referred in reference [5–9]. However, the lack of global accuracy and other shortcomings such as size effects and mesh-dependency problems limit the development of finite element method. It is wildly accepted that spectral method takes advantage in precision. Theoretically, the infinite order accuracy can be achieved by solving the

M. Abdel Wahab (Ed.): NME 2018, LNME, pp. 104–113, 2019.
https://doi.org/10.1007/978-981-13-2273-0_9

continuous function problem through spectral method. Wang did some research of SMA via Chebyshev spectral method [10–12].

In actual conditions, Chebyshev spectral method and Legendre spectral method are wildly used to solve the engineering problem with complex boundary conditions due to their excellent performance. However, both of these spectral method have fatal drawback for that these methods' calculations are too complex. Besides, Chebyshev method is unstable in the numerical simulation of the boundary region due to its weight function. Legendre method is more stable than Chebyshev method, but its computational complexity is even worse. If a discontinuous function is solved by normal spectral method, it may not be correctly modeled [13]. The appearance of Legendre wavelets method [13] makes things better. Wavelets analysis has many useful properties to solve the problems mentioned above [14]. This new method takes both advantages of Legendre method and wavelets method, and its computational complexity is much better than normal Legendre method.

In the current paper, the microstructure of 1-D SMA model is simulated via Legendre wavelets method for both statics and dynamics conditions at a certain temperature. A dimensionless form is carried out to finish the simulations. The analysis of phase transformation in these situation is presented as well. The advantage of Legendre wavelets method to reduce calculation is proven. The current paper is organized as follows. The mathematical model of SMA is presented in Sect. 2. An introduction of Legendre wavelets is given in Sect. 3. Finally, the simulations and analysis are discussed in Sect. 4 and Sect. 5. Concluding remarks are given in Sect. 6.

2 Mathematical Model for SMA

Considering the fundamental laws, energy balance and so on, the basic equation for the mechanical wave interactions of the 1-D isothermal SMA dynamic model used in the current paper is listed as follows [15]:

$$\rho u_{tt} = \sigma_x + f. \tag{1}$$

According to the Landau theory, the relationship between stress σ and strain ε can be described as follow:

$$\sigma = k_1(\theta - \theta_1)\varepsilon + k_2\varepsilon^3 + k_3\varepsilon^5, \tag{2}$$

where strain $\varepsilon = \frac{\partial u}{\partial x}$, constants k_1, k_2, k_3 denote Landau coefficients. Taking into account the internal friction effect with a Rayleigh dissipation term and the domain wall energy term, Eq. (1) can be rewritten as:

$$\rho u_{tt} = \sigma_x + v\frac{\partial}{\partial t}\frac{\partial^2 u}{\partial x^2} - k_g\frac{\partial^4 u}{\partial x^4} + f. \tag{3}$$

Thus, the governing function of isothermal model for the first order martensitic phase transformations in a 1-D microstructure [4] can be described as follows:

$$\begin{array}{l} \rho u_{tt} = \sigma_x + v\frac{\partial}{\partial t}\frac{\partial^2 u}{\partial x^2} - k_g\frac{\partial^4 u}{\partial x^4} + f \\ \sigma = k_1(\theta - \theta_1)\varepsilon + k_2\varepsilon^3 + k_3\varepsilon^5 \end{array}, \tag{4}$$

with the boundary condition:

$$\begin{array}{ll} u(0) = 0, & u(L) = 0, \\ \left.\frac{\partial^2 u}{\partial x^2}\right|_{x=0} = 0, & \left.\frac{\partial^2 u}{\partial x^2}\right|_{x=L} = 0. \end{array} \tag{5}$$

where k_1, k_2, k_3 are constants of materials, k_g is the Ginzburg coefficient which should be relatively small compared to k_1, v is the coefficient of internal friction, ρ is the density, and f is the mechanical loading. Taking into account the static condition which means the terms involving time derivative equal zero, Eq. (4) can be written as an ordinary differential equation (ODE) form:

$$k_1(\theta - \theta_1)\frac{\partial^2 u}{\partial x^2} + k_2\left(\frac{\partial u}{\partial x}\right)^2\frac{\partial^2 u}{\partial x^2} + k_3\left(\frac{\partial u}{\partial x}\right)^4\frac{\partial^2 u}{\partial x^2} - k_g\frac{\partial^4 u}{\partial x^4} + f = 0, \tag{6}$$

with the same boundary conditions in (5).

3 Numerical Algorithm via Legendre Wavelets

Wavelets are functions constructed using the expansion and translation of the mother wavelet function, and they are always orthogonal functions. The mother wavelet function of the Legendre wavelets are derived from Legendre polynomials [16]. The general family of Legendre wavelets retains the following form:

$$\psi_{n,m}(x) = \begin{cases} \sqrt{m+\frac{1}{2}}2^{\frac{k}{2}}P_m\left(2^k x - 2n + 1\right), & for\ \frac{n-1}{2^{k-1}} \le x \le \frac{n}{2^{k-1}}, \\ 0, & otherwise \end{cases} \tag{7}$$

where $m = 0, 1, \ldots, M-1, n = 1, 2, 3, \ldots, 2^{k-1}$, $\sqrt{m+\frac{1}{2}}$ is the coefficient for orthogonality. $P_m(x)$ here are the Legendre polynomials with order m.

A function $f(x)$ defined in interval [0, 1] can be expanded as Legendre wavelets in the following form:

$$f(x) = \sum_{n=1}^{\infty}\sum_{m=0}^{\infty} c_{n,m}\psi_{n,m}(x) = C^T\Psi(x). \tag{8}$$

When $f(x)$ is truncated, Eq. (8) can be rewritten as

$$f(x) = \sum_{n=1}^{2^{k-1}} \sum_{m=0}^{M-1} c_{n,m}\psi_{n,m}(x) = C^T \Psi(x), \tag{9}$$

where

$$C = [c_{10}, c_{11}, \ldots, c_{M-1}, c_{20}, \ldots, c_{2M-1}, \ldots, c_{2^{k-1}0}, \ldots, c_{2^{k-1}M-1}]^T, \tag{10}$$

and

$$\Psi(x) = [\psi_{10}(x), \ldots, \psi_{M-1}(x), \psi_{20}(x), \ldots, \psi_{2M-1}(x), \ldots, \psi_{2^{k-1}0}(x), \ldots, \psi_{2^{k-1}M-1}(x)]^T. \tag{11}$$

3.1 Operational Matrix of Derivative

In the current paper, the calculation of derivative in spectral space is performed as an operational matrix form [16]:

$$\frac{\mathrm{d}\Psi(x)}{\mathrm{dx}} = D\Psi(x), \tag{12}$$

where D is a $2^k M \times 2^k M$ operational matrix defined as:

$$\mathrm{D} = \begin{pmatrix} F & 0 & \cdots & 0 \\ 0 & F & & 0 \\ \vdots & & \ddots & \vdots \\ 0 & 0 & \cdots & F \end{pmatrix}, \tag{13}$$

where F is a $M \times M$ matrix which is defined as:

$$\mathrm{F}_{r,s} = \begin{cases} 2^{k+1}\sqrt{(2r-1)(2s-1)}, r = 2, \ldots, M, S = 1, \ldots, r-1, \textit{ and } (r+s)\textit{ odd}, \\ 0, \quad \textit{otherwise}. \end{cases} \tag{14}$$

The vector C in Eq. (10) is called the spectral space coefficient in calculation, and this coefficient can be applied to calculate the derivative by multiplying the matrix D.

3.2 Numerical Algorithm

The system (4) can be recast in the following form:

$$\begin{gathered} \frac{\partial u}{\partial t} = V, \frac{\partial^2 u}{\partial x^2} = \mathrm{w}, \\ \rho \frac{\partial V}{\partial t} = \sigma_x + v \frac{\partial^2 V}{\partial x^2} - k_g \frac{\partial^2 w}{\partial x^2} + f, \\ \sigma = k_1(\theta - \theta_1)\frac{\partial u}{\partial x} - k_2\left(\frac{\partial u}{\partial x}\right)^3 + k_3\left(\frac{\partial u}{\partial x}\right)^5. \end{gathered} \tag{15}$$

The boundary condition can be described as:

$$\begin{gathered} u(0) = 0, \quad u(L) = 0, \\ w(0) = 0, \quad w(L) = 0. \end{gathered} \tag{16}$$

By employing the Legendre wavelets method, the given set of differential equations in (15) can be concerted into ODEs. The last equation of (15) is also discretized using Legendre wavelets method, which become a set of algebraic equations. By combining ODEs and algebraic equations, the system (15) can be rewritten in the following form:

$$L\frac{dU}{dt} + N(t, x, U) = 0, \tag{17}$$

where L is the matrix of linear operator, N is the matrix of nonlinear operator and $U = [u, V, w, \sigma]^T$. The stiff system (17) needs to be solved through an implicit algorithm. The backward differentiation formula is applied here to discretize the time derivative:

$$L(U^n - U^{n-1}) + \Delta t N(t, x, U^n) = 0, \tag{18}$$

where n is the current time layer. For each layer, iterations are performed by using Newton's method. The iterative stopping criterion is that the relative residual is less than $1e^{-5}$.

4 Numerical Simulation

The numerical experiments data employed in the current paper were published in [11], which were for a $Au_{23}Cu_{30}Zn_{47}$ rod:
$k_1 = 480\,\mathrm{g/(ms^2cmK)}$, $k_2 = 6 \times 10^6\,\mathrm{g/(ms^2cmK)}$, $k_3 = 4.5 \times 10^8\,\mathrm{g/(ms^2cmK)}$,
$\theta_1 = 208$ K, $\theta = 240$ K, $\rho = 11.1\,\mathrm{g/cm^3}$, $k_g = 10$ g/((cm)(ms)),
All the simulations were taken in the Matlab2015a.

4.1 Dimensionless Form of the Governing Equations

The equations in (15) are rescaled into a dimensionless form by using the following change of variables [17]:

$$\varepsilon = \varepsilon_0 \tilde{\varepsilon}, x = \delta \tilde{x}, t = t_0 \tilde{t}, \tag{19}$$

with $\varepsilon_0 = \sqrt{\frac{k_2}{k_3}}$, $\delta = \frac{\sqrt{k_g k_3}}{k_2}$, $t_0 = \frac{\sqrt{\rho k_g} k_3}{k_2^2}$.

The mechanical field Eq. (15) now can be rescaled as follows:

$$\begin{gathered} \frac{\partial \tilde{u}}{\partial \tilde{t}} = \tilde{V}, \frac{\partial^2 \tilde{u}}{\partial \tilde{x}^2} = \tilde{w}, \\ \frac{\partial \tilde{V}}{\partial \tilde{t}} = \widetilde{\sigma_{\tilde{x}}} + \tilde{v} \frac{\partial^2 \tilde{V}}{\partial \tilde{x}^2} - \frac{\partial^2 \tilde{w}}{\partial \tilde{x}^2} + \tilde{f}, \\ \tilde{\sigma} = \tilde{k}(\theta - \theta_1)\tilde{\varepsilon} - \tilde{\varepsilon}^3 + \tilde{\varepsilon}^5. \end{gathered} \tag{20}$$

There are many advantages to rescale the equations into a dimensionless form, such as simplifying the calculations and improving numerical stability.

4.2 Simulation Results of the Static Equation

In this section, the simulation is performed using the condition of $k = 3$ and $M = 6$ in Sect. 3. The dimensionless form of the governing equations can be got from Eq. (19) in 4.1:

$$\begin{gathered} \sigma_{\tilde{x}} = \frac{\partial^4 \tilde{u}}{\partial \tilde{x}^4} - \tilde{f}, \\ \sigma = \widetilde{k_1}\, \tilde{\varepsilon} + \tilde{\varepsilon}^3 + \tilde{\varepsilon}^5, \end{gathered} \tag{21}$$

where $\tilde{f} = 0.4$, $\tilde{\varepsilon} = \frac{\partial \tilde{u}}{\partial \tilde{x}}$.

In this simulation, the new temperature-dependent coefficient $\widetilde{k_1}$ was set to 0.192, which means the temperature was set to $240^{\circ} K$. Thus, the initial condition should begin from the austenitic phase:

$$\widetilde{u_0(x)} = 0. \tag{22}$$

Newton method was applied to complete this simulation with the derivative matrix in Sect. 3.1. Figure 1 (left) shows the figure of displacement $\tilde{u}$. Figure 1 (right) shows the figure of strain $\tilde{\varepsilon}$. Under this mechanical loading, it can be obtained from Fig. 1 that the SMA rod has finally finished the phase transformation into the martensitic phase. And the results are in line with expectations.

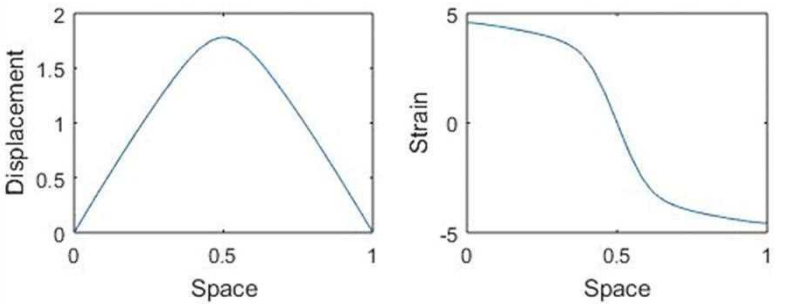

Fig. 1. The simulation results of static system.

4.3 Simulation Results of the Dynamic Equation

In this section, the simulation is performed using the dynamic condition of the coefficients $k = 3$ and $M = 6$ in Sect. 3. Equation (19) in 4.1 is the dimensionless form of the governing equations. The time step in this experiment is set as $\Delta\tilde{t} = 1 \times 10^{-4}$. The initial value is given by Eq. (21).

The dimensionless mechanical loading that changes over time is defined as

$$\tilde{f} = 0.4\sin^3(4\pi t). \tag{23}$$

Under this mechanical loading, the SMA rod should switch between martensitic phase and austenite phase. In this section, the temperature is set to $250^{\circ}K$. The mechanical and temperature initial conditions make sure that both martensitic and austenitic phase can exist. And the free energy function here has two local minima, which correspond to twins martensitic phase, and one minimum that corresponds to austenite phase. The simulation results are presented in Fig. 2. It is shown that the austenite phase transforms into twins martensitic phase when the absolute value of loading exceed the certain value. Therefore, the phase transformations here are induced by the applied mechanical loading.

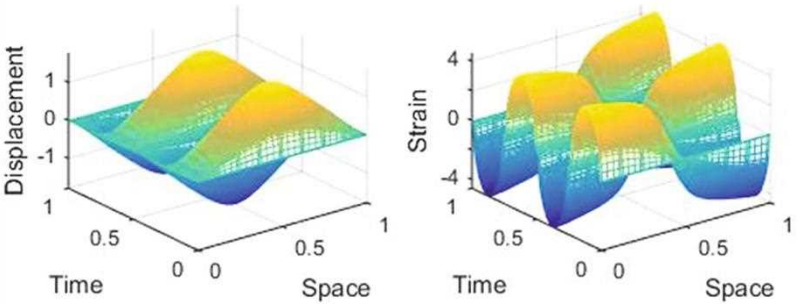

Fig. 2. The simulation result of dynamics system.

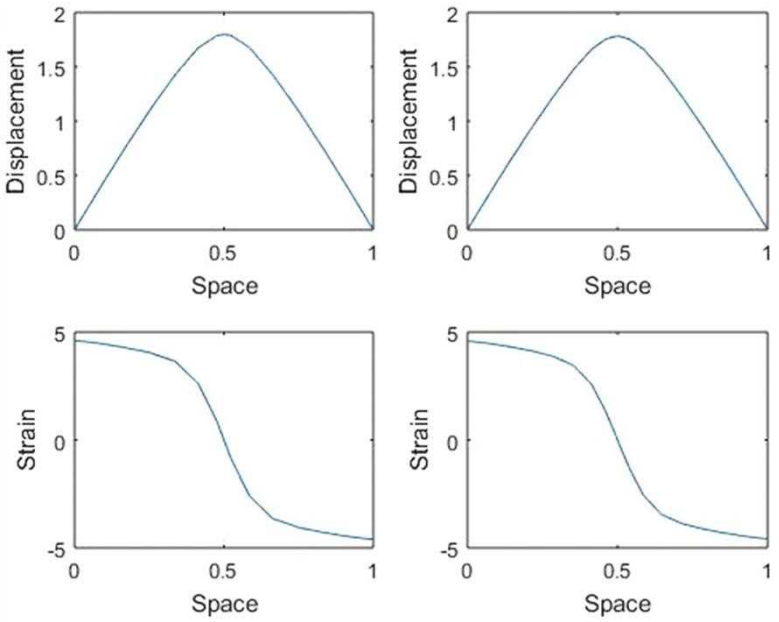

Fig. 3. The simulation results of static system. (left) k = 2, M = 6; (right) k = 1, M = 12.

5 Convergence Analysis

In this section, the numerical simulations are performed in matlab2015a with Intel i5-6500 CPU and 8 GB RAM. The static model is used to analyze the convergence rate of the algorithm proposed in the current paper with different grid points. The coefficient k and M in this section is just the same as these in Sect. 3. Two experiments are presented in this section to prove that our algorithm can reduce the amount of calculation.

The first experiment is taken to compare the difference between two grids which are k = 2, M = 6 and k = 1, M = 12. The total number of points for both grids is 24. Figure 3 shows the results of this simulation. It is observed that the accurateness of two results are almost the same. However, the time spent by these experiments is hugely different. The simulation of k = 2, M = 6 only needs 111.05 s to get the accurateness of 10^{-3}, but the other one takes 428.53 s to complete the same work.

The second experiment is taken to compare the difference between two grids which are k = 2, M = 6 and k = 3, M = 6. The second grid has the same number of points in one interval as the first grid, but the number of intervals is twice that of the first one. Figure 4 shows the results of this simulation. It is observed that the accurateness of the second grid with the coefficients k = 3, M = 6 are much better than the first grid with the coefficients k = 2, M = 6. However, the second gird takes almost the same time as the first one to finish the work.

Table 1 shows the time for each gird to obtain the certain tolerance error with the norm $\left\|L\frac{dU}{dt}+N(t,x,U)\right\|_2$. It is evident from this table that the time spent increases

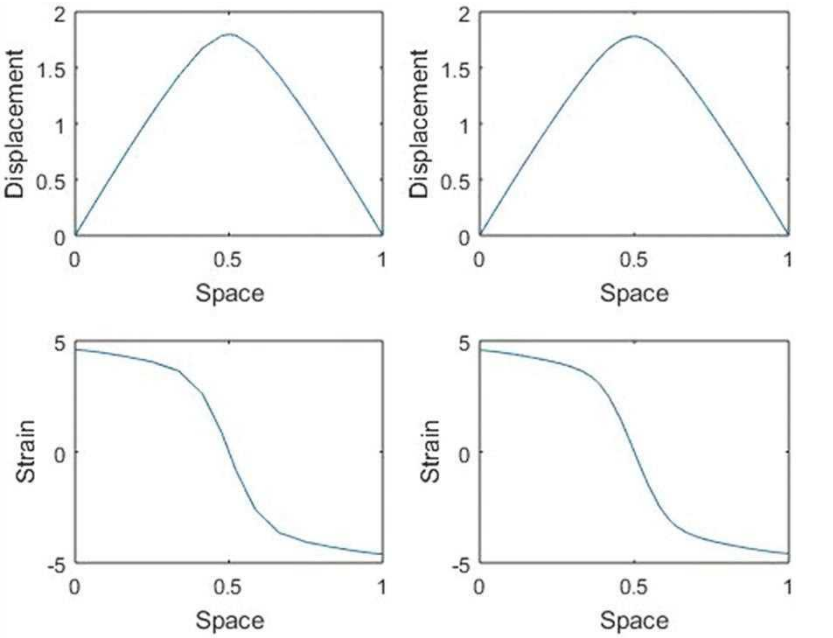

Fig. 4. The simulation results of static system. (left) k = 2, M = 6; (right) k = 3, M = 6.

Table 1. The calculation time with different grids and accurateness.

	10^{-1}	10^{-2}	10^{-3}
k = 2, M = 6	80.34 s	93.40 s	111.05 s
k = 3, M = 6	84.61 s	99.57 s	116.52 s
k = 1, M = 12	383.14 s	400.78 s	428.53 s
k = 2, M = 12	384.77 s	402.74 s	429.18 s

significantly with the increase of the M value, however it is not sensitive to the change of k. So the calculation time can be reduced by controlling the number of points in one interval and increasing the number of intervals appropriately. Thus, it is obviously to see that wavelets method has a great advantage of reducing calculation.

6 Conclusion

In the current paper, an isothermal model has been proposed to simulate the 1-D microstructure of SMA. The mechanically induced phase transformation process in both static and dynamic systems has been successfully simulated via Legendre wavelets method. The entire numerical algorithm for Legendre wavelets method to solve the partial differential equation has been described in detail in the current paper. The Legendre wavelets method's advantage of reducing calculation has been verified

by the control experiments under static condition. The efficiency of spectral method to solve microstructure problem has been improved at the mathematical level.

Acknowledgements. This work has been supported by the National Natural Science Foundation of China (Grant No. 51575478 and Grant No. 61571007), the National Sciences and Engineering Research Council (NSERC) of Canada, and the Canada Research Chair Program.

References

1. Ölander, A.: An electrochemical investigation of solid cadmium-gold alloys. Am. Chem. Soc. **54**, 3819–3833 (1932)
2. Vernon, L.B., Vernon, H.M.: Process of manufacturing articles of thermoplastic synthetic resins. In: US Patent 2234993 (1941)
3. Wu, M.H., Schetky, L.M.: Industrial applications for shape memory alloys. In: International Conference on Shape Memory and Superelastic Technologies. Pacific Grove, California, USA, pp. 171–182 (2000)
4. Leo, D.J., Weddle, C., Naganathan, G., Buckley, S.J.: Vehicular applications of smart material systems. pp. 106–116 (1998)
5. Hartl, D.J., Lagoudas, D.C.: Aerospace applications of shape memory alloys. Proc. Inst. Mech. Eng., Part G: J. Aerosp. Eng. **221**, 535–552 (2007)
6. Lagoudas, D., Hartl, D., Chemisky, Y., et al.: Constitutive model for the numerical analysis of phase transformation in polycrystalline shape memory alloys. Int. J. Plast **32–33**(2), 155–183 (2012)
7. Patoor, E., Lagoudas, D.C., Entchev, P.B., et al.: Shape memory alloys, part I: general properties and modeling of single crystals. Mech. Mater. **38**(5–6), 391–429 (2006)
8. Lagoudas, D.C., Entchev, P.B., Popov, P., et al.: Shape memory alloys, part ii: modeling of polycrystals. Mech. Mater. **38**(5–6), 430–462 (2006)
9. Hartl, D.J., Chatzigeorgiou, G., Lagoudas, D.C.: Three-dimensional modeling and numerical analysis of rate-dependent irrecoverable deformation in shape memory alloys. Int. J. Plast **26** (10), 1485–1507 (2010)
10. Wang, L.X., Melnik, R.V.N.: Simulation of phase combinations in shape memory alloys patches by hybrid optimization methods. Appl. Numer. Math. **58**(4), 511–524 (2008)
11. Wang, L.X., Melnik, R.V.N.: Thermo-mechanical wave propagation in shape memory alloy rod with phase transformations. Mech. Adv. Mater. Struct. **14**(8), 665–676 (2007)
12. Wang, L.X., Melnik, R.V.N.: Numerical model for vibration damping resulting from the first order phase transformations. Appl. Math. Model. **31**, 2008–2018 (2007)
13. Razzaghi, M., Yousefi, S.: Legendre wavelets method for the solution of nonlinear problems in the calculus of variations. Math. Comput. Model. **34**(1–2), 45–54 (2001)
14. Ming, Q., Hwang, C., Shih, Y.P.: The computation of wavelet-galerkin approximation on a bounded Interval. Int. J. Numer. Methods Eng. **39**, 2921–2944 (1996)
15. Wang, L.X., Melnik, R.V.N.: Finite volume analysis of nonlinear thermo-mechanical dynamics of shape memory alloys. Heat Mass Transfer **43**, 535–546 (2007)
16. Mohammadi, F., Hosseini, M.M.: A new legendre wavelet operational matrix of derivative and its applications in solving the singular ordinary differential equations. J. Franklin Inst. **348**(8), 1787–1796 (2011)
17. Dhote, R.P., Melnik, R.V.N., Zu, J.: Dynamic thermo-mechanical coupling and size effects in finite shape memory alloy nanostructures. Comput. Mater. Sci. **63**, 105–117 (2012)

Magd Abdel Wahab
Editor

Proceedings of the 1st International Conference on Numerical Modelling in Engineering

Volume 2: Numerical Modelling in Mechanical and Materials Engineering, NME 2018, 28–29 August 2018, Ghent University, Belgium

Springer

Editor
Magd Abdel Wahab
Faculty of Engineering and Architecture
Ghent University, Laboratory Soete
Ghent, Belgium

ISSN 2195-4356 ISSN 2195-4364 (electronic)
Lecture Notes in Mechanical Engineering
ISBN 978-981-13-2272-3 ISBN 978-981-13-2273-0 (eBook)
https://doi.org/10.1007/978-981-13-2273-0

Library of Congress Control Number: 2018952641

This Springer imprint is published by the registered company Springer Nature Singapore Pte Ltd.
The registered company address is: 152 Beach Road, #21-01/04 Gateway East, Singapore 189721, Singapore